Supporting Information

Design of High-Performance Antimony / MXene Hybrid Electrodes for Sodium-Ion Batteries

Stefanie Arnold,[1,2] Antonio Gentile,[3,4] Yunjie Li,[1,2] Qingsong Wang,[1,5] Stefano Marchionna,[4] Riccardo Ruffo,[3,6*] and Volker Presser[1,2,7*]

[1] INM - Leibniz Institute for New Materials, Campus D2.2, 66123 Saarbrücken, Germany

[2] Department of Materials Science and Engineering, Saarland University, Campus D2.266123 Saarbrücken, Germany

[3] Dipartimento di Scienza dei Materiali, Università degli Studi di Milano Bicocca, Via Cozzi 55, 20125 Milano, Italy

[4] Ricerca sul Sistema Energetico- RSE S.p.A., Via R. Rubattino 54, 20134 Milano, Italy

[5] Institute of Nanotechnology, Karlsruhe Institute of Technology, Hermann-von-Helmholtz-Platz 1, 76344, Eggenstein-Leopoldshafen, Germany

[6] National Reference Center for Electrochemical Energy Storage (GISEL) - Consorzio Interuniversitario Nazionale per la Scienza e Tecnologia dei Materiali (INSTM), 50121 Firenze, Italy

[7] Saarene - Saarland Center for Energy Materials and Sustainability, Campus D4.2, 66123 Saarbrücken, Germany

* Corresponding author's E-Mail: VP: volker.presser@leibniz-inm.de; RR: riccardo.ruffo@unimib.it

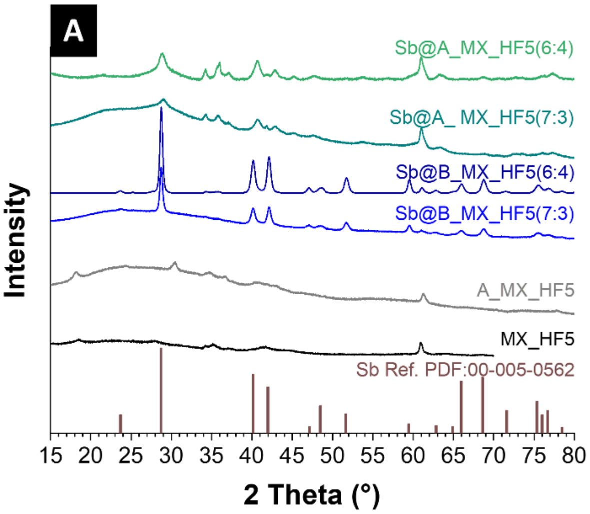

Figure S1: X-ray diffraction patterns of different Sb@$Ti_3C_2T_z$ hybrid materials (+pure $Ti_3C_2T_z$ and expanded $Ti_3C_2T_z$) by using the MXene etched with 5 mass% HF (**A**) and 30 mass% HF (**B**).

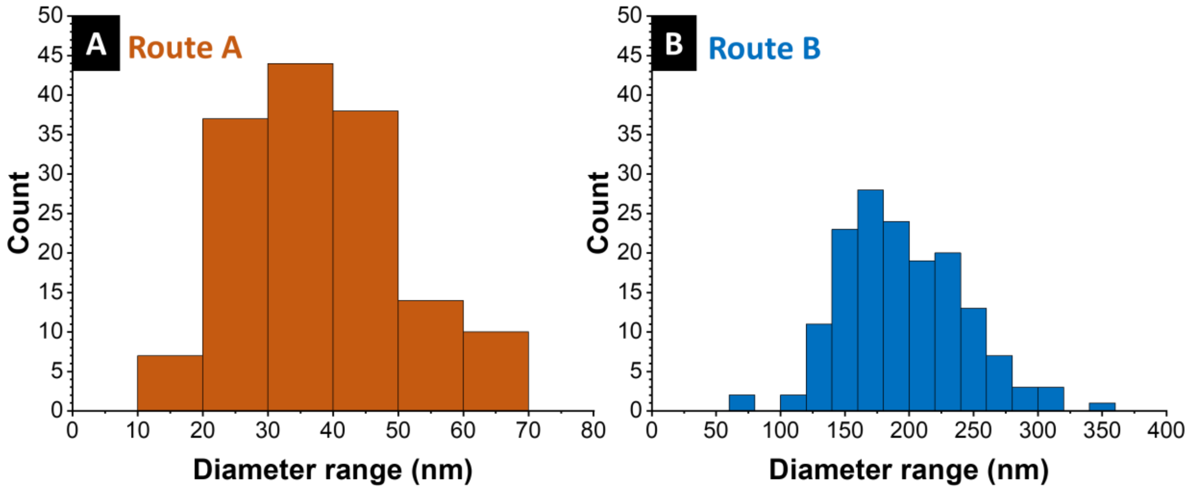

Figure S2: Particle size distribution derived from image analysis of scanning electron micrographs of 150 antimony particles synthesized via synthesis Route A (**A**) and via synthesis Route B (**B**).

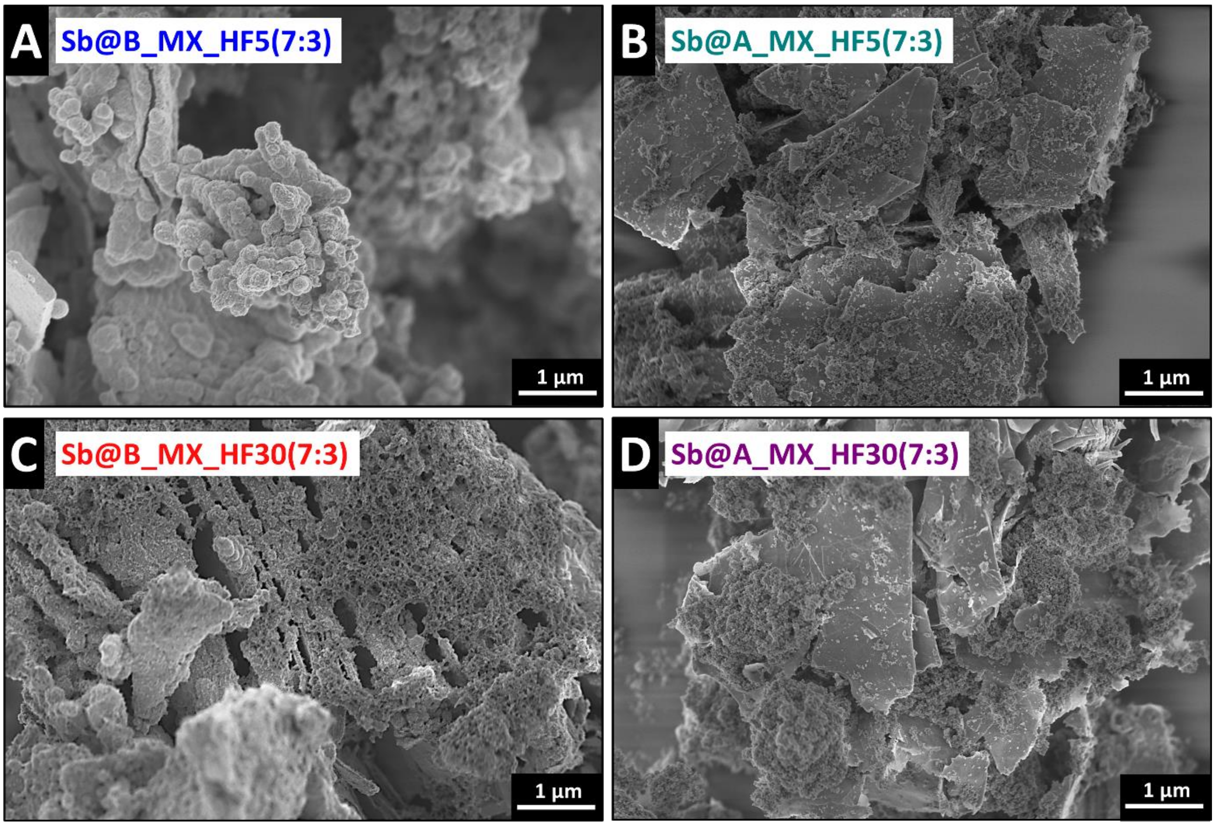

Figure S3: Scanning electron micrographs of (**A**) antimony $Ti_3C_2T_z$ (5 mass% HF) hybrid with a composition of 7:3 (**B**) antimony expanded $Ti_3C_2T_z$ (5 mass% HF) hybrid with a composition of 7:3 (**C**) antimony $Ti_3C_2T_z$ (30 mass% HF) hybrid with a composition of 7:3 (**D**) antimony expanded $Ti_3C_2T_z$ (30 mass% HF) hybrid with a composition of 7:3.

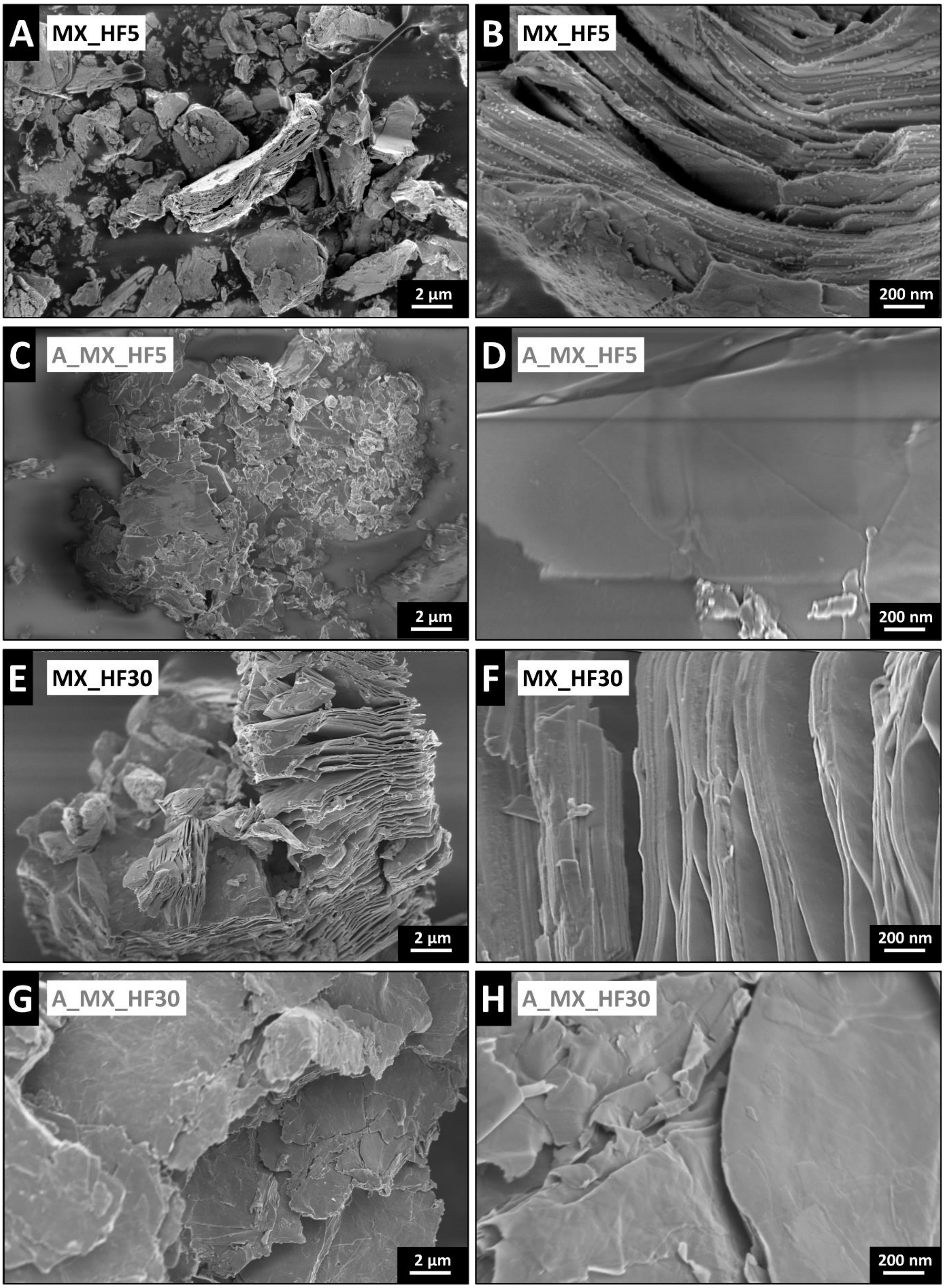

Figure S4: Material characterization of the different MXenes. Scanning electron micrographs of (**A-B**) $Ti_3C_2T_z$ (5 mass% HF), (**C-D**) with TMAOH expanded $Ti_3C_2T_z$ (5 mass% HF), (**E-F**) $Ti_3C_2T_z$ (30 mass% HF), (**G-H**) with TMAOH expanded $Ti_3C_2T_z$ (30 mass% HF).

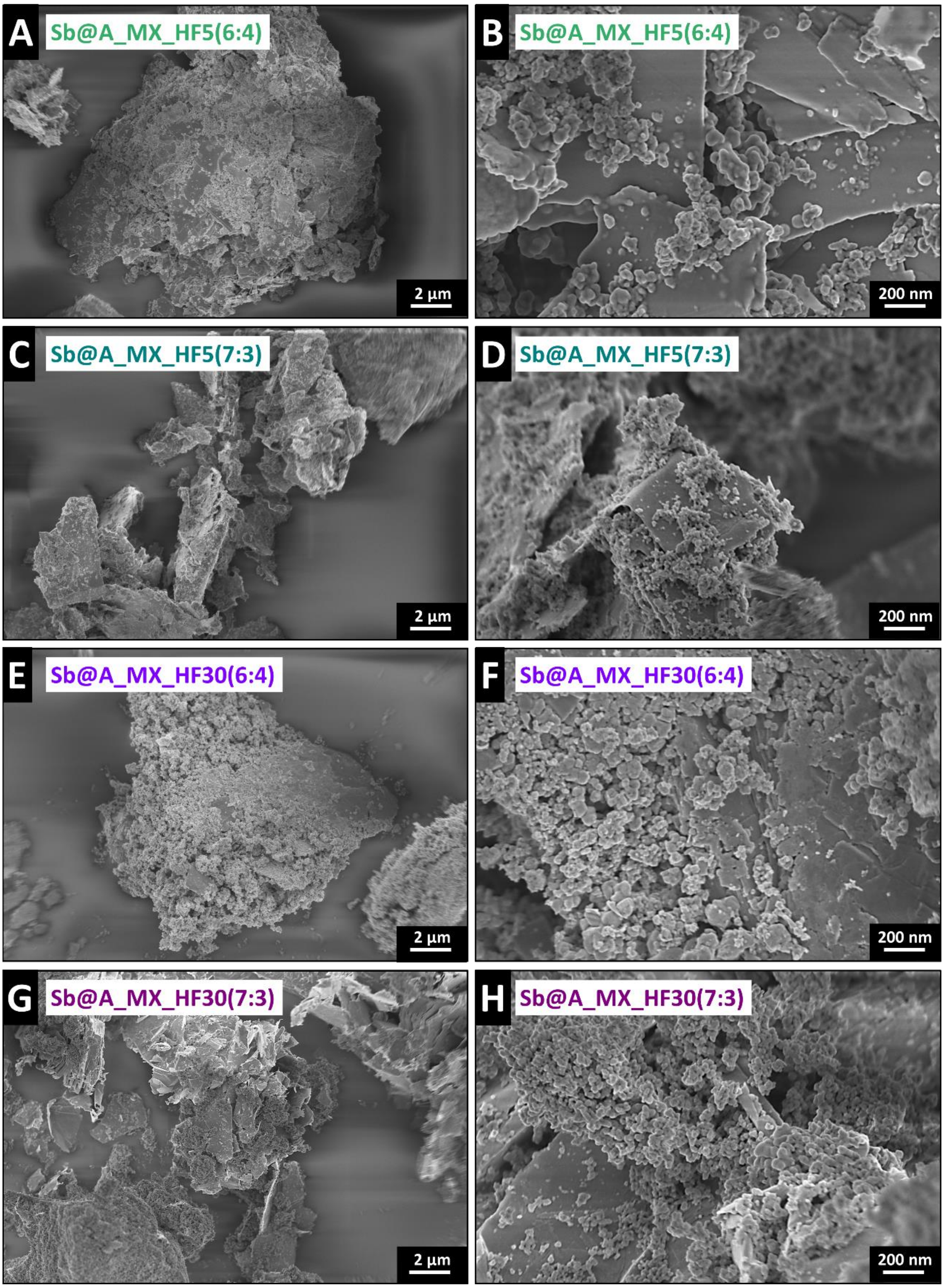

Figure S5: Material characterization of the different with TMAOH expanded MXene antimony hybrids. Scanning electron micrographs of (**A-B**) antimony expanded $Ti_3C_2T_z$ (5 mass% HF) hybrid with a composition of 6:4, (**C-D**) antimony expanded $Ti_3C_2T_z$ (5 mass% HF) hybrid with a composition of 7:3, (**E-F**) antimony expanded $Ti_3C_2T_z$ (30 mass% HF) hybrid with a composition of 6:4, (**G-H**) antimony expanded $Ti_3C_2T_z$ (30 mass% HF) hybrid with a composition of 7:3.

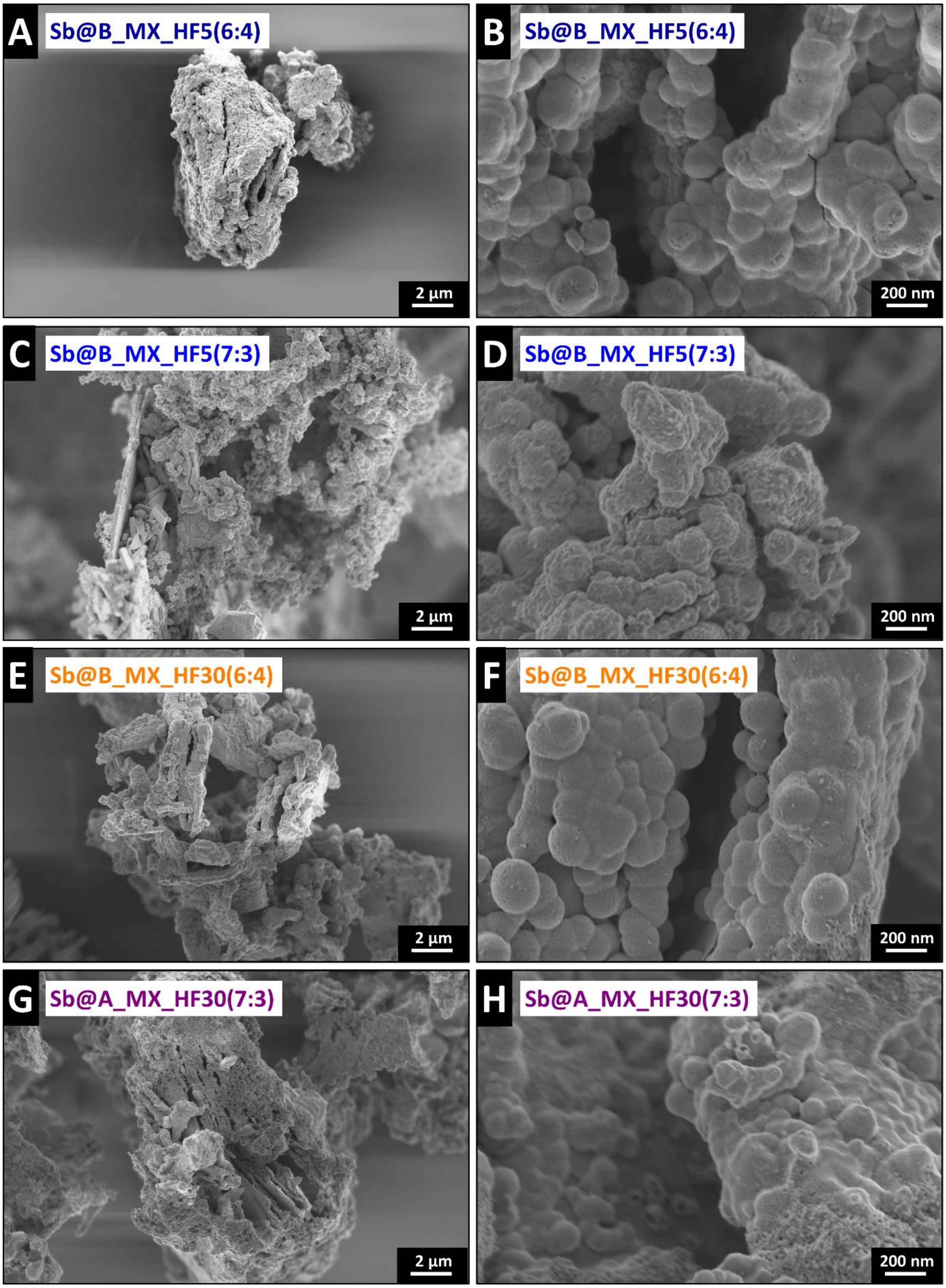

Figure S6: Material characterization of the different MXenes hybrids. Scanning electron micrographs of (**A-B**) antimony $Ti_3C_2T_z$ (5% mass% HF) hybrid with a composition of 6:4, (**C-D**) antimony $Ti_3C_2T_z$ (5% mass% HF) hybrid with a composition of 7:3, (**E-F**) antimony $Ti_3C_2T_z$ (30% mass% HF) hybrid with a composition of 6:4, (**G-H**) antimony $Ti_3C_2T_z$ (30% mass% HF) hybrid with a composition of 7:3.

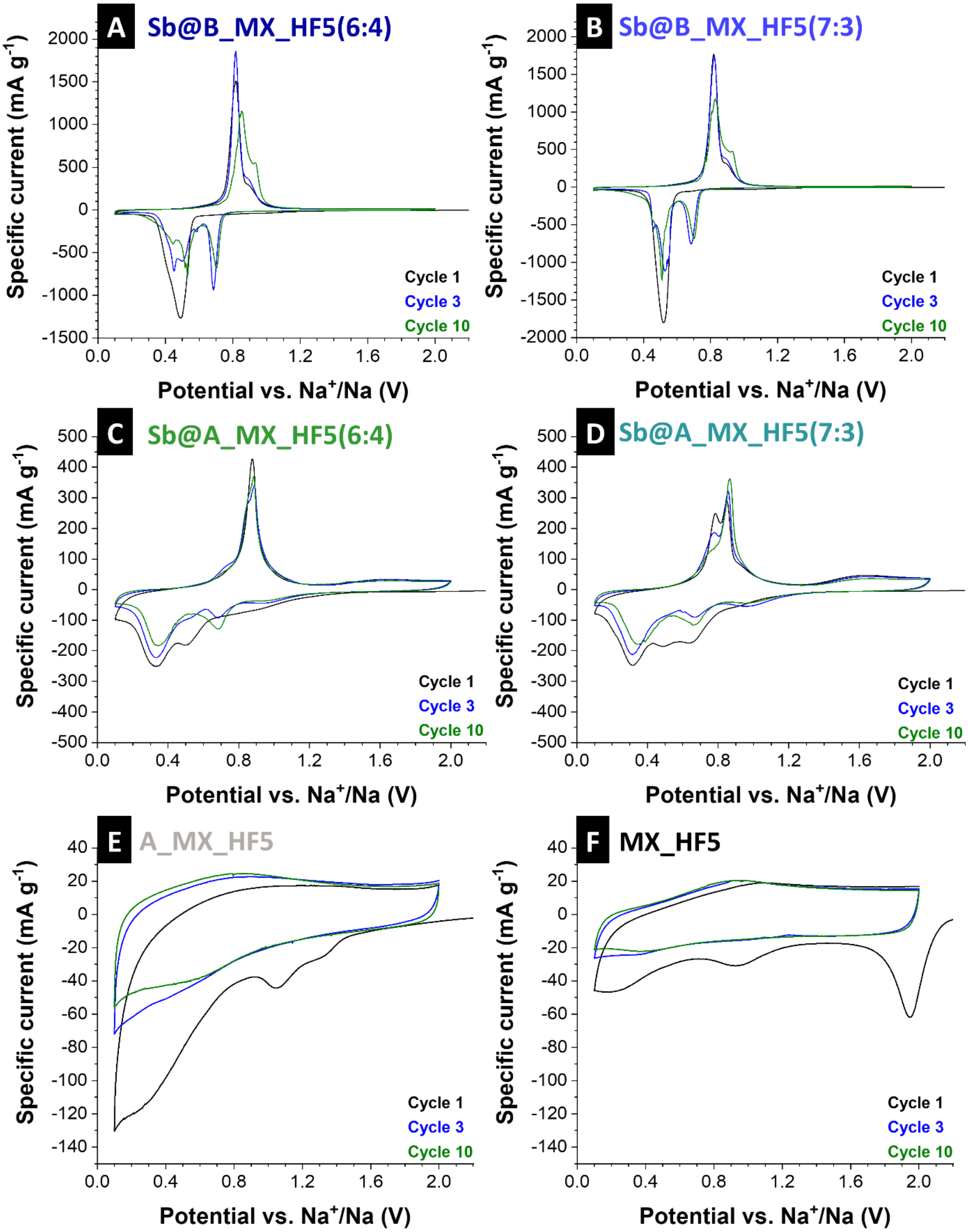

Figure S7: Cyclic voltammograms recorded at 0.1 mV s^{-1} in the potential range of 0.1-2.0 V vs. Na^+/Na for (**A**) antimony $Ti_3C_2T_z$ (5% mass% HF) hybrid with a composition of 6:4, (**B**) antimony $Ti_3C_2T_z$ (5% mass% HF) hybrid with a composition of 7:3, (**C**) antimony expanded $Ti_3C_2T_z$ (5% HF) hybrid with a composition of 6:4, (**D**) antimony expanded $Ti_3C_2T_z$ (5% mass% HF) hybrid with a composition of 7:3, (**E**) v $Ti_3C_2T_z$ (5% mass% HF), (**F**) not expanded $Ti_3C_2T_z$ (5% mass% HF).

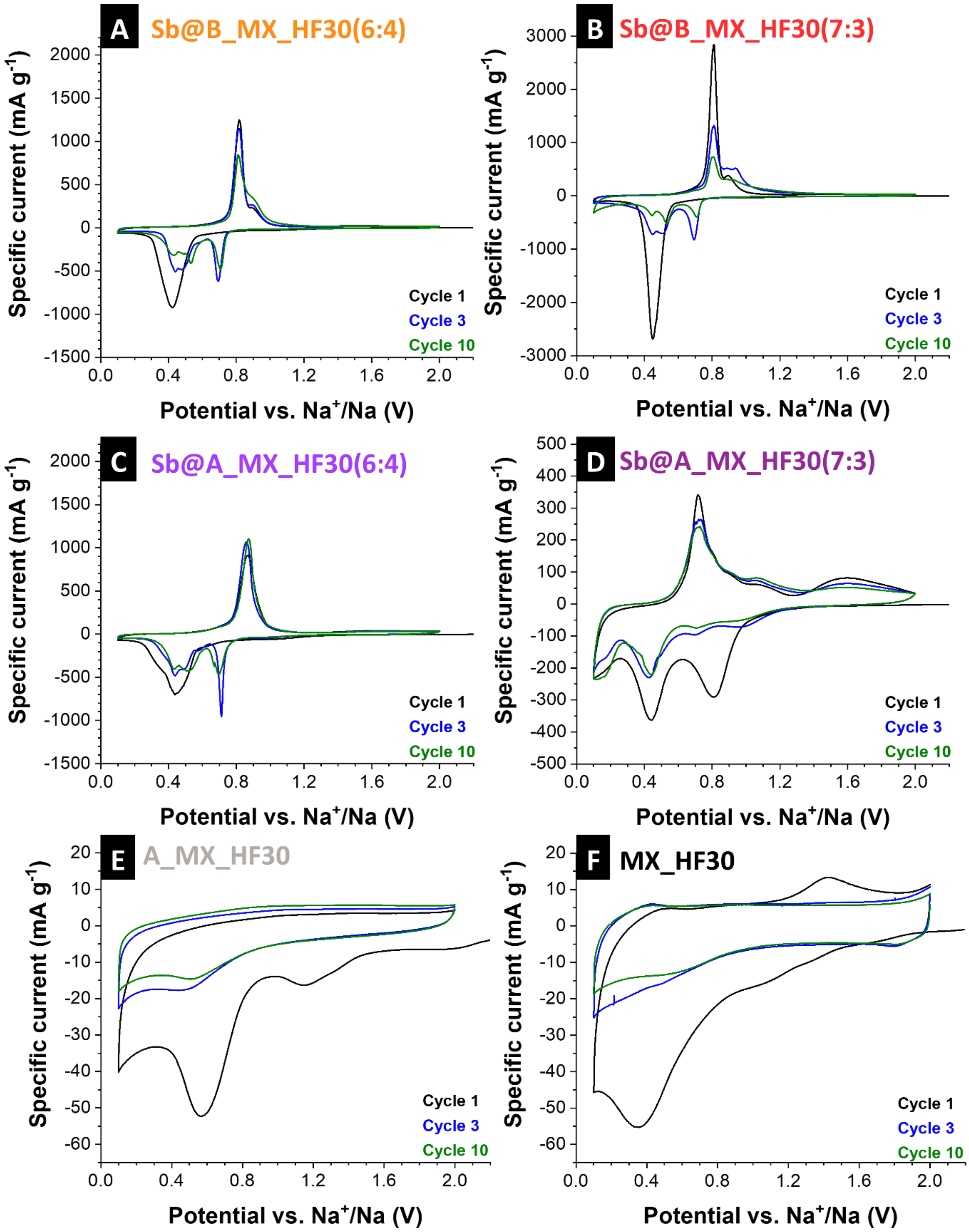

Figure S8: Cyclic voltammograms recorded at 0.1 mV s^{-1} in the potential range of 0.1-2.0 V vs. Na^+/Na for (**A**) antimony $Ti_3C_2T_z$ (30% mass% HF) hybrid with a composition of 6:4, (**B**) antimony $Ti_3C_2T_z$ (30% mass% HF) hybrid with a composition of 7:3, (**C**) antimony expanded $Ti_3C_2T_z$ (30% mass% HF) hybrid with a composition of 6:4, (**D**) antimony expanded $Ti_3C_2T_z$ (30% mass% HF) hybrid with a composition of 7:3, (**E**) expanded $Ti_3C_2T_z$ (30% mass% HF), (**F**) not expanded $Ti_3C_2T_z$ (30% mass% HF).

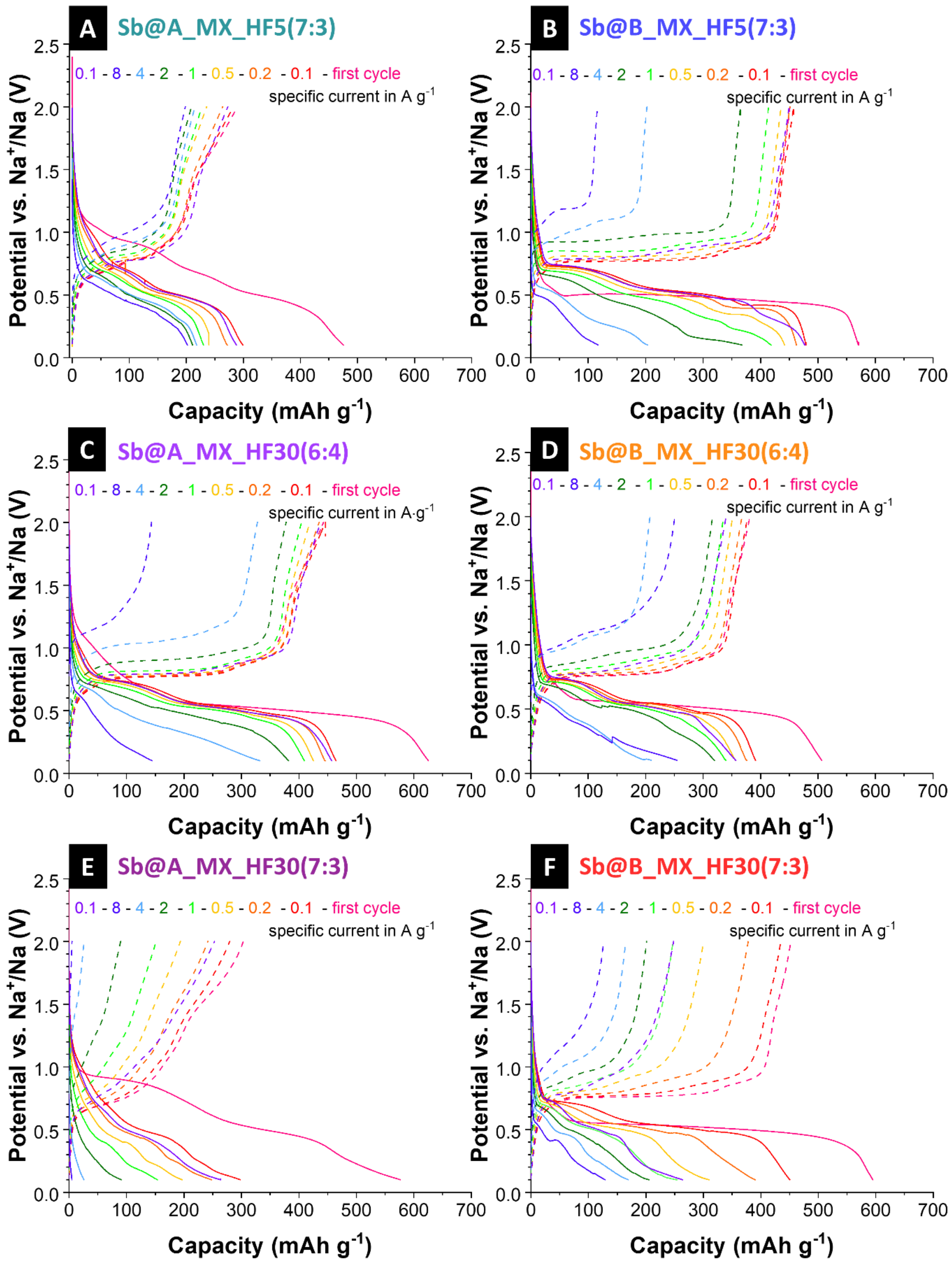

Figure S9: Galvanostatic charge and discharge profiles at different applied specific currents of 0.1-8 A g^{-1} between 1.0 V and 3.0 V *vs.* Na^+/Na of (**A**) Sb@A_MX_HF5(7:3), (**B**) Sb@B_MX_HF5(7:3), (**C**) Sb@A_MX_HF30(6:4), (**D**) Sb@B_MX_HF30(6:4), (**E**) Sb@A_MX_HF30(7:3), and (**F**) Sb@B_MX_HF30(7:3).

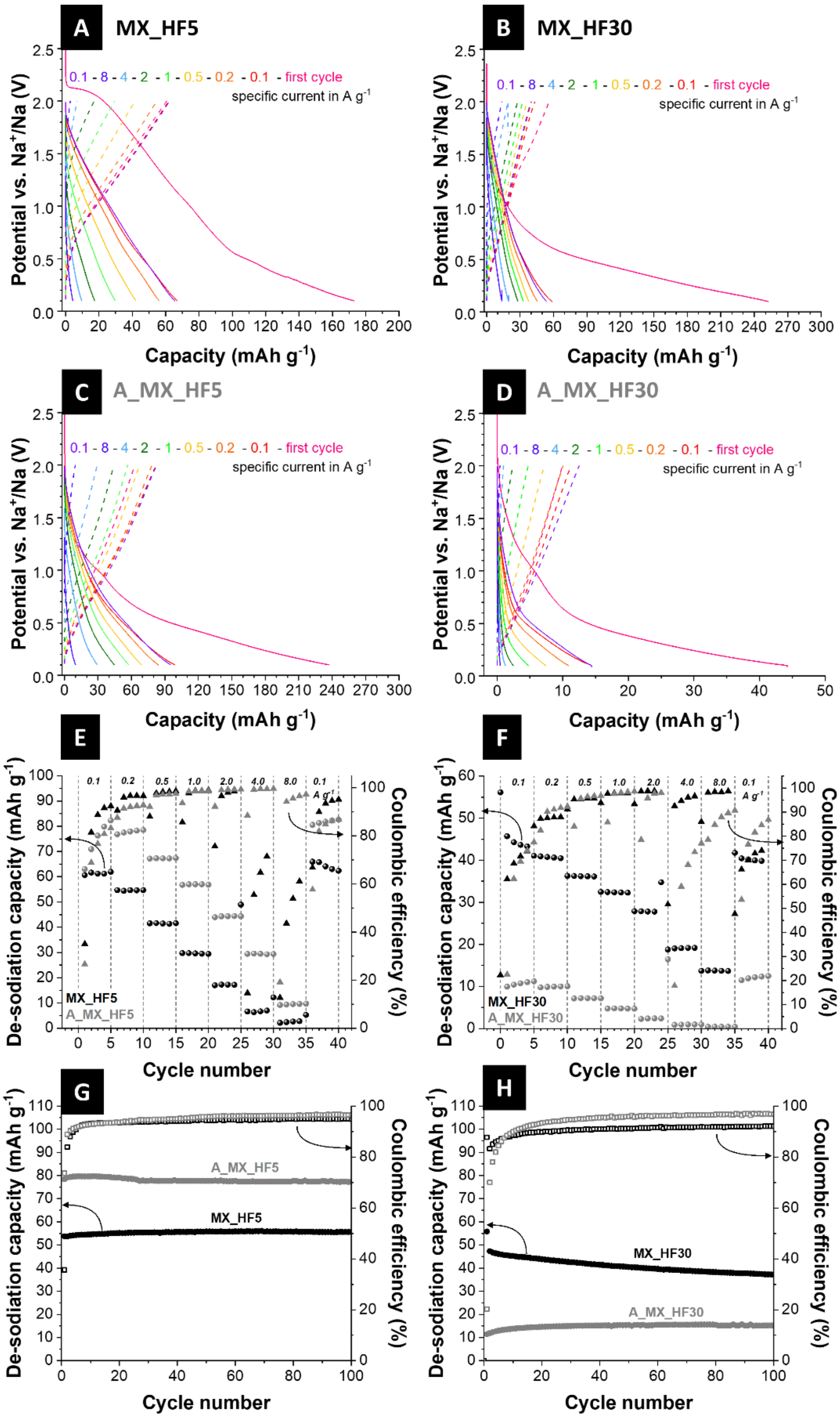

Figure S10: Electrochemical characterization of the non-expanded and expanded $Ti_3C_2T_z$, etched with 5 mass% HF. Galvanostatic charge and discharge profiles at rates of 0.1-8 A g^{-1} (1.0-3.0 V vs. Na^+/Na) of (**A**) MX_HF5, (**B**) MX_HF30, (**C**) A_MX_HF5, and (**D**) A_MX_HF30. Rate performance using galvanostatic charge/discharge cycling and Coulombic efficiency values at different rates for (**E**) MX_HF5 and A_ MX_HF5, (**F**) MX_HF30 and A_MX_HF30. Galvanostatic charge/discharge cycling stability and Coulombic efficiency values at a specific current of 0.1 A g^{-1} for (**G**) MX_HF5 and A_MX_HF5, (**H**) MX_HF30 and A_MX_HF30.

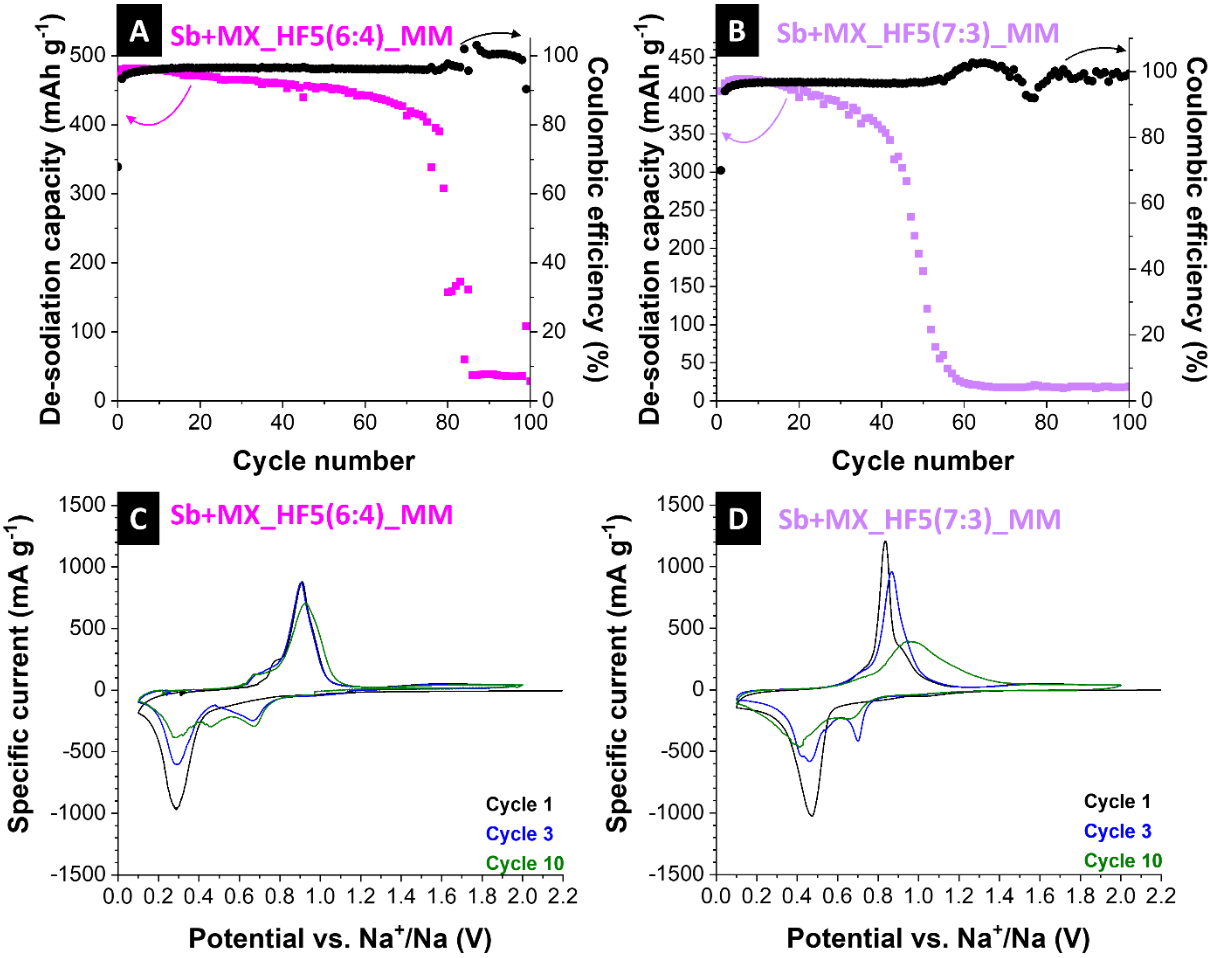

Figure S11: Galvanostatic charge/discharge cycling performance electrochemical stability with corresponding Coulombic efficiency values at a specific current of 0.1 A g^{-1} for (**A**) Sb+MX_HF5(6:4)_MM, and (**B**) Sb+MX_HF5(7:3)_MM. Cyclic voltammograms recorded at a rate of 0.1 mV s^{-1} in the potential range of 0.1-2.0 V vs. Na^+/Na for (**C**) Sb+MX_HF5(6:4)_MM, and (**D**) Sb+MX_HF5(7:3)_MM.

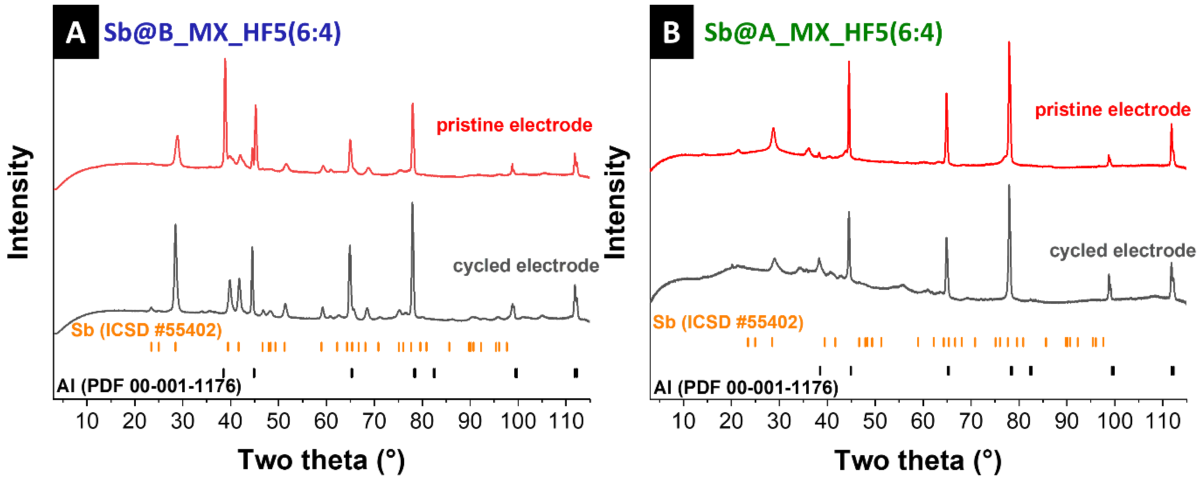

Figure S12: X-ray diffraction pattern of (**A**) pristine and post mortem Sb@B_MX_HF5(6:4) electrode (**B**) pristine and cycled Sb@A_MX_HF5(6:4) electrode. The diffraction patterns were recorded with the setup XRD-2 (see Experimental).

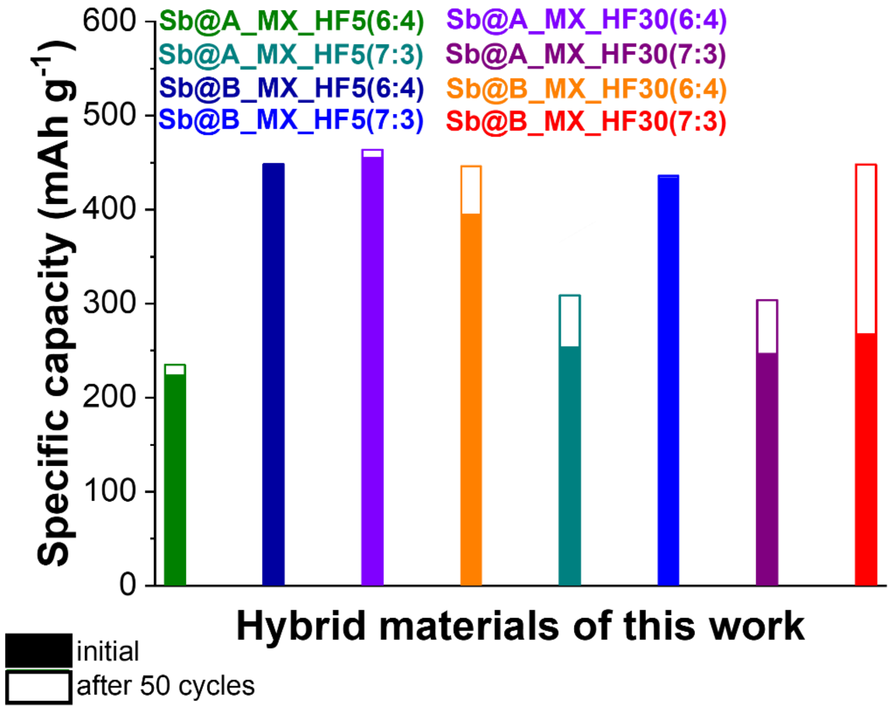

Figure S13: Graphical illustration and overview of initial specific capacities as well as values after 50 cycles of cycling at a specific current of 0.1 A g^{-1} of all hybrid antimony MXene hybrid materials produced in this work.